Functionalization of iron oxide/mesoporous silica core-shell nanoparticles for removal of rare earth elements

Fižulić, Valentina

Master's thesis / Diplomski rad

2019

Degree Grantor / Ustanova koja je dodijelila akademski / stručni stupanj: **University of Zagreb, Faculty of Food Technology and Biotechnology / Sveučilište u Zagrebu, Prehrambeno-biotehnološki fakultet**

Permanent link / Trajna poveznica: https://urn.nsk.hr/urn:nbn:hr:159:895987

Rights / Prava: In copyright/Zaštićeno autorskim pravom.

Download date / Datum preuzimanja: **2025-02-18**

UNIVERSITY OF ZAGREB

FACULTY OF FOOD TECHNOLOGY AND BIOTECHNOLOGY

GRADUATE THESIS

Zagreb, July 2019

Valentina Fižulić

1020/MB

FUNCTIONALIZATION OF IRON OXIDE/MESOPOROUS SILICA CORE-SHELL NANOPARTICLES FOR REMOVAL OF RARE EARTH ELEMENTS

FUNCTIONALIZATION OF IRON OXIDE/MESOPOROUS SILICA CORE-SHELL NANOPARTICLES FOR REMOVAL OF RARE EARTH ELEMENTS

Valentina Fižulić, 0058204643

Abstract: *Rare earth elements (REEs) are a group of 17 chemically similar elements with unique magnetic, optical and catalytic properties which make them non-substitutable in modern green and advanced technologies. Growing demand for these elements as well as their limited resources led to development of technologies for recovery of REEs from various waste sources. The aim of this thesis was to synthesize and functionalize magnetic nanoparticles which could be potentialy used in recovering of REEs from aqueous solutions. Products of two different protocols for obtaining iron oxide nanoparticles were compared and used in synthesis of iron oxide/mesoporous silica core-shell nanoparticles as magnetic cores. Moreover, core-shell nanoparticles were functionalised with diethylenetriaminepentaacetic acid. Synthesized nanoparticles were characterized by infrared spectroscopy, dynamic light scattering, transmission electron microscopy and thermogravimetric analyses*

Université d'Orléans - Université de Zagreb

U. F. R. Faculté des Sciences - Faculté de Nutrition et Biotechnologie - Faculté des Sciences

MASTER SCIENCES et TECHNOLOGIE

mention**: Biologie-Biochimie**

spécialité: **Techniques Bio-Industrielles**

Stage report

Functionalization of iron oxide/mesoporous silica core-shell nanoparticles for removal of rare earth elements

by

VALENTINA FIŽULIĆ

(February, 2019 – June, 2019)

Organisation: Institut Charles Gerhardt (ICGM), équipe "Ingénierie Moléculaire et Nano Objets"

Place of the stage: Montpellier, France

Supervisor of the stage: Dr. Jean-Olivier Durand

Referees: Dr. Laurence Raehm and doc.dr.sc. Filip Šupljika

Date of defense: 1st July 2019

Abstract

Rare earth elements (REEs) are a group of 17 chemically similar elements with unique magnetic, optical and catalytic properties which make them non-substitutable in modern green and advanced technologies. Growing demand for these elements as well as their limited resources led to development of technologies for recovery of REEs from various waste sources.

The aim of this thesis was to synthesize and functionalize magnetic nanoparticles which could be potentialy used in recovering of REEs from aqueous solutions. Products of two different protocols for obtaining iron oxide nanoparticles were compared and used in synthesis of iron oxide/mesoporous silica core-shell nanoparticles as magnetic cores. Moreover, core-shell nanoparticles were functionalised with diethylenetriaminepentaacetic acid. Synthesized nanoparticles were characterized by infrared spectroscopy, dynamic light scattering, transmission electron microscopy and thermogravimetric analyses.

Key words: nanoparticles,   iron   oxide,   core-shell,   mesoporous   silica, diethylenetriaminepentaacetic acid, rare earth elements

Résumé

Les terres rare (REEs) forment un groupe de 17 éléments chimiques possédant des propriétés magnétiques, optiques et catalytiques uniques qui les rendent non substituables dans les technologies modernes vertes et avancées. La demande croissante pour ces éléments ainsi que leur ressource limitée amènent au développement de technologies pour le recyclage des REEs présents dans les eaux usées.

Le but de cette thèse de master a été de synthétiser et fonctionnaliser des nanoparticules magnétiques qui pourraient être utilisées dans le cadre de recyclage des REEs présents dans les solutions aqueuses. Les nanoparticules d'oxide de fer issues de deux protocoles différents ont été comparées et utilisées comme cœurs magnétiques pour la synthèse de cœur-coquille oxide de fer-silice mésoporeuse. De plus, les nanoparticules de cœur-coquille ont été fonctionalisés avec de l'acide diethylentriaminepentaacetic. Les nanoparticules synthétisées furent caractérisées par spectroscopie infra-rouge, diffusion dynamique de la lumière (DLS), microscopie électronique à transmission et analyse thermogravimétrique.

Mots clés: nanoparticules, oxide de fer, cœur-coquilles, silice mésoporeuse, acide diethylentriaminepentaacetic, terres rare

ACKNOWLEDGMENTS

First of all, I would like to express my sincere gratitude to my supervisor, Dr. Jean-Olivier Durand, who gave me an opportunity to learn and work in such a stimulating environment and who helped me tremendously during my stay in France.

I would like to give my special thanks to Dr. Mathilde Ménard, without whom all of this wouldn't be possible. She guided me during my internship, equipped me with knowledge and, most importantly, provided me with precious advices along the way.

I would also like to thank prof.dr.sc. Vladimir Mrša, prof.dr.sc. Višnja Bessendorfer, prof. Chantal Pichon and prof.emer. Daniel Hagége who gave us an opportunity to grow in professional, as well as personal, way by organizing this programme.

Finally, I would like to thank my family and friends who believed in me even when I didn't. Without their love and support, I wouldn't be where I am today.

Contents

1. INTRODUCTION

1.1. Recovery of rare earth elements from aqueous solutions

Rare earth elements (REEs) is a joint name for a group of 17 chemically similar elements - 15 lanthanides (lanthanum, cerium, praseodymium, neodymium, promethium, samarium, europium, gadolinium, terbium, dysprosium, holmium, erbium, thulium, ytterbium and lutetium), scandium and yttrium. This group if further devided to light (La, Ce, Pr and Nd), middle (Sm, Eu and Gd) and heavy (Tb, Dy, Ho, Er, Tm, Yb, Lu and Y) rare earths (Zhanheng, 2011; Yanfei et al., 2016).

In the years following their discovery, which was in 1788 in Ytterby, Sweden, REEs had only been found in few other places so it was thought that they were rare, hence the name (Abraham, 2011). In reality, REE are relatively abundant in the Earth's crust but their extraction is in general challenging, environmentally unfriendly and expensive (Zhou, 2017). Due to the low labor costs and flexible environmental regulatory policies, China was able to offer REEs at low prices which other countries couldn't compete with. That led China to become the lead producer and exporter of REEs (UNCTAD, 2014). In 2005, China decided to reduce its annual export quotas of REEs which caused the rising of prices and even shortage of some REEs in following years. That was why companies began exploring new possible sources of these elements with unique magnetic, optical and catalytic properties (Zhou et al., 2016). This uniqueness is exactly why REEs are non-substitutable in new-emerging technologies (high-tech applications, e.g. hybrid cars, mobile phones, wind turbines, fluorescent lights) and are still used in traditional sectors such as agriculture, metallurgy, petroleum and textile (Chen and Zheng, 2019).

Growing demand as well as the fact that these elements pollute the environment upon their disposal led to the development of technologies for recovery of REEs from the various waste sources such as ores, end-of-life consumer products and wastewater (Swain and Mishra, 2019; Binnemans and Jones, 2015). Many methods have been employed for separation, purification and pre-contentration of the REEs including chemical precipitation, liquid-liquid extraction, ion exchange and adsorption. Due to its simplicity, high efficiency and wide-range availability, adsorption is one of the most interesting methods today (Anastopoulos et al., 2016).

Nanomaterials have an advantage in wastewater treatment over conventional materials thanks to their high surface areas, higher efficiency and faster adsorption rate (Sadegh et al., 2017). Surface of nanomaterials can be functionalised in order to increase their selectivity and $Fe_3O_4/\gamma–Fe_2O_3$ can be introduced to said sorbent to ease the separation of nanomaterials after the treatment by applying an external magnetic field (Guo et al., 2015).

1.2. Magnetic iron oxide nanoparticles

Iron oxide is a common mineral compound which can either be found in nature or synthesised in laboratory. Among eight known types of iron oxides (Cornell and Shwertmann, 2003), hematite (α-Fe_2O_3), magnetite (Fe_3O_4) and maghemite (γ-Fe_2O_3), christallographically presented in Figure 1, are most commonly used due to their suitability for various technical and biomedical applications. Hematite is the most frequent and very stable polymorph but has weak ferromagnetic or antiferromagnetic properties at room temperature. On the other hand, magnetite and maghemite are easily magnetized. Magnetite is probably the most interesting of the three because it can be present in a form of different polymorphs with each of them having unique magnetic properties (Campos et al., 2015).
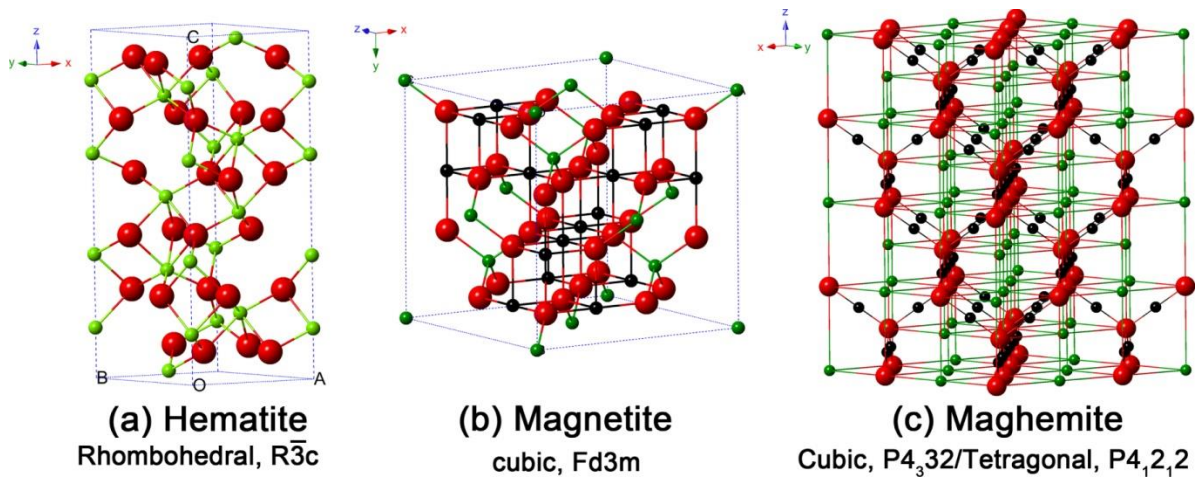

Figure 1. Crystal structure and crystallographic data of the hematite, magnetite and maghemite (the black ball is Fe^{2+}, the green ball is Fe^{3+} and the red ball is O^{2-}) (Wu et al., 2015)

Iron oxide nanoparticles (IO NPs) can be obtained through various different methods such as co-precipitation, thermal decomposition, hydrothermal and solvothermal syntheses, sol-gel synthesis, microwave-assisted synthesis, microemulsion, etc. High-temperature thermal decomposition is a non-aqueous synthesis which consists in decomposing metallic compounds (e.g. iron (II) stearate (Ménard, 2017)., iron (III) oxide (Dib et al., 2014), iron (III) acetylacetonate (Knežević et al., 2017; Li et al., 2010; Guardia et al., 2014), in high boiling point organic solvents in the presence of stabilizing surfactants (Arias et al., 2018). Organic molecules such as oleic acid, oleylamine, 1-tetradecene, and 1-octadecene can act as stabilizers and are used to obtain monodisperse IO NPs. Stabilizer molecules decelerate nucleation process and the growing of nanocrystals. This may lead to formation of small nanoparticles (Wu et al., 2015). For obtaining larger nanocrystals, dibenzyl ether is often used because its decomposition generates molecules with active role in the control of the size and nucleation of the nanocrystals. Guardia et al. (2014) reported poor reproducibility of the process unless squalane is added. This solvent has a high boiling point which helps in smoothening temperature fluctuations that are result of dibenzyl ether decomposition. By adjusting the ratio of these two solvents, nanocrystals of various sizes can be obtained. If oleic acid is used in the process of thermal decomposition, these molecules will adsorb onto the surface of the synthesized IO NPs by chemisorption in a form of monolayer of oleic acid molecules (Zhang et al., 2006). This coating increases stability of iron oxide nanoparticles and allows their dispersibility only in organic solvents (e.g. chloroform).

1.3. Mesoporous silica nanoparticles with magnetic cores

To prevent aggregation of IO NPs, which is caused by the interparticle hydrophobic interactions, and leaching of iron ions in aqueous solutions, coating step must be performed. The most commonly used compound for this purpose is silica. Silica has many advantages as it is nontoxic, mechanically stable and chemically inert material and when used as coating provides high number of silanol groups on its surface which can be used for grafting of different ligands.

To synthesize iron oxide/mesoporous silica nanoparticles (IO@MS NPs), mesoporous meaning containing pores from 2-50 nm in diameter, sol-gel process can be used. IO NPs coated with stabilizing ligand (usually oleic acid) and dispersed in oil phase (usually chloroform) need

to be transfered into water as the coating step is performed in aqueous phase. To create oil-in-water microemulsion, the solution of IO NPs needs to be added to an aqueous solution of surfactant (the most commonly used is cetyltrimethylammonium bromide, CTAB) under vigorous stirring. Then, the oil phase is evaporated by heating of the solution at 80ºC for approximately 10 min in order to transfer IO NPs into the aqueous phase. The transfer is driven by the hydrophobic van der Waals interactions between the alkyl chains of the stabilizing ligand, oleic acid, and the ones of the surfactant, CTAB. The role of surfactant molecules is to reduce repulsion between hydrophobic IO NPs and water. This results in interdigitated bilayer structures on IO NP's surface which are stable in water (Fan et al., 2004; Fan et al., 2005a; Fan et al., 2005b). Surfactant also acts as a soft organic template for the growth of a mesoporous silica layer on the surface of the IO NPs. Generally, silica coating of IO NPs is performed under basic conditions. Under these conditions, silanol groups of the silica source (e.g. tetraethyl orthosilicate, TEOS) are partially deprotonated. Thus, these negatively charged groups can interact with cationic surfactant (e.g. CTAB) (Owens et al., 2016). In other words, basic conditions cause hydrolyzation of silica precursors and condensation of silica onto the surface of the IO NP.
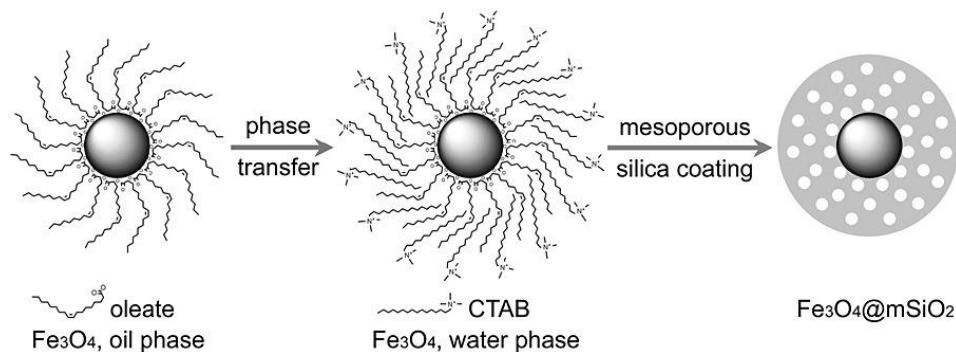

Figure 2. Schematic illustration of the procedure for synthesis of mesoporous silica/iron oxide core–shell nanoparticles (Ye et al., 2012)

It is important to mention that thickness of the silica shell, as well as size of its porosity, can be tuned. It was shown that the increase of [CTAB]/[IO NPs] and [H2O]/[CTAB] ratios

allowed hydrolyzation and condensation of the higher amount of TEOS around iron oxide core which consequently led to an increased thickness of the silica shell. Moreover, if the concentration of the CTAB is too high, it leads to the production of nanoparticles without cores. On the other hand, if the concentration is too low, thickness of the core-shell nanoparticles does not increase even if the TEOS was added in excess (Ye et al., 2012). Zhang et al. (2008) demonstrated that by using cationic surfactants (alkyltrimethilammonium bromides) with different hydrocarbon chain lengths, pore sizes in silica shell can be tuned. Their results indicated correlation of hydrocarbon chain lengths (C_{14}, C_{16} and C_{18}) and obtained pore sizes (2.4 nm, 2.8 nm and 3.4 nm respecitvely). After the sol-gel process, CTAB has to be removed in order to free the porosities IO@MS NPs and because of its cytotoxicity (Wang et al., 2008).

1.4. Functionalization of silica nanoparticles

As stated above, silica nanoparticles can have a wide number of applications depending on their surface modifications. Silica surface is covered with silanol and siloxane groups. Silanol groups provide the hydrophilic properties to silica nanoparticles and can be functionalised either by electrostatic coupling or by covalent ligands (Nyalosaso et al., 2016).

Surface activation of silica consists in hydrolyzation of silane alkoxy groups to silanol groups and their condenzation with the hydroxyl groups on silica surface result in stable Si-O-Si covalent bonds (Bruce and Sen, 2005). Different solvents, temperatures and drying methods are used to perform silanization. Alkoxysilanes can contain different functional groups such as amino, vinyl, epoxy, etc. (Florea et al., 2013) (3-aminopropyl)trietoxysilane (APTES) is one of the most used aminosilanes and one of the prefered coupling agents for silica because of its bifunctionality. Disadvantage of APTES is that it can interact with the silica surface in more than one way (Figure 3) with some of the interactions being weak (Figure 3c-e) and some resulting in low silane grafting density (Figure 1b) (Zhu et al., 2012).
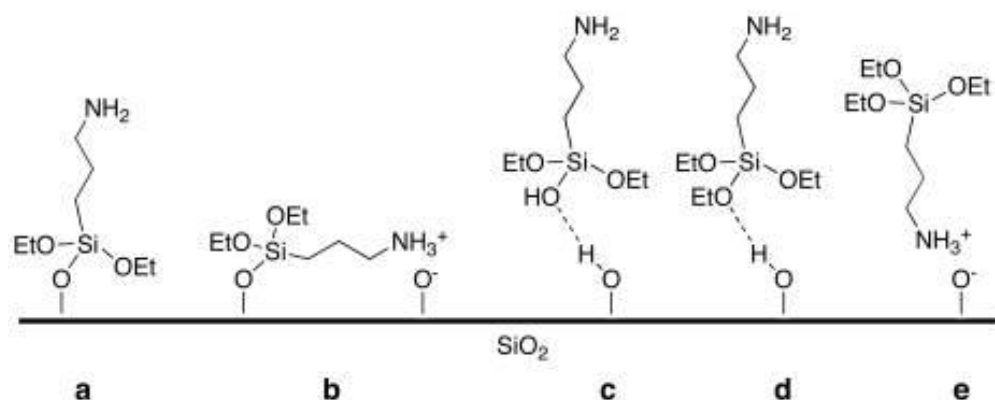
Figure 3. Different types of interactions between APTES molecules and silicon dioxide substrates: (a) a covalently attached APTES molecule with its amine group extending away from the interface, (b) a covalently attached APTES molecule with its amine group interacting with a surface silanol group, and (c)–(e) weakly bounded APTES molecules (Zhu et al., 2012)

Diethylenetriaminepentaacetic acid (DTPA) is an aminopolycarbosilic acid that acts as a octadentate chelating agent. DTPA can be used for functionalization of the silica nanoparticles by first grafting APTES on the surface and then introducing DTPA dianhydride. It was previously demonstrated by Dib et al. (2014) that DTPA-functionalised magnetic mesoporous nanocontainers can remove heavy metals from aqueous solutions. Regarding the REEs, DTPA functionalised chitosan-silica hybrid materials showed different affinity for the adsorption of lanthanide ions ($La^{3+} < Nd^{3+} < Lu^{3+} < Eu^{3+} < Dy^{3+}$) (Roosen et al., 2014). Ashour et al. (2018) showed similar results with DTPA-functionalised silica microparticles ($La^{3+} < Ce^{3+} < Pr^{3+} < Nd^{3+} < Y^{3+} < Dy^{3+}$) and nanoparticles ($La^{3+} < Nd^{3+} < Dy^{3+}$). According to these results, it can be concluded that DTPA may have higher affinity to heavy REEs. Callura et al. (2018) demonstrated that the adsorbtion of the REEs was most effective in acidic solutions for DTPA dianhydride-functionalised silica microparticles. They also showed that uptake of REEs generally isn't affected by the presence of competing ions in solution which indicates the selectivity of this ligand for REEs.

2. MATERIALS AND METHODS

2.1. Materials

Hydrated iron (III) oxide (catalyst grade 30-50 mesh), oleic acid (90%), cetyltrimethylammonum bromide (≥99%), tetraethyl orthosilicate (≥99%), ammonium nitrate (≥98%), diethylenetriaminepentaacetic dianhydride (98%) and (3-aminopropyl)trietoxysilane (99%) were purchased from Sigma-Aldrich. Oleylamine (approximate C18 content 80-90%) and n-docosane (99%) were purchased from Acros. Dimethylformamide (≥99%), diethyl ether (≥99,5%) and n-pentane (≥99%) were purchased from Fisher Chemical. Ethanol (96% and absolute), ethyl acetate (99,9%) and sodium hydroxide (99%) were purchased from VWR. Iron (II) stereate (9% Fe) was purchased from Strem Chemicals. Acetone (≥99%) was purchased from Honeywell. Chloroform (≥99,8%) was purchased from CARLO ERBA Reagents. Triethylamine (≥99%), dibenzyl ether (≥98%) and squalane (≥98,5%) were purchased from Merck Milipore.

2.2. Equipment and analysis

Infrared (IR) spectroscopy is an instrumental method used for identification of functional groups in a sample and/or monitoring the changes in sample composition (e.g. monitoring of the washing steps). Result of the analysis is visualised as an IR spectrum which consists of multiple absorption bands. As each functional group provides characteristic absorption band(s) (in terms of intensity and frequency) when analysed with IR spectrometry, the composition of analysed sample can be indentified by proper identification of absorption bands in IR spectrum. Monitoring of the washing steps of IO NPs, IO@MS NPs and grafting of ligand onto the IO@MS NPs was performed using the PerkinElmer Sprectrum Two FTIR spectrophotometer.

Dynamic light scattering (DLS) is a technique used for particle size analysis in nanometer range which is based on the Brownian motion theory, theory that the disprsed particles are moving individually and randomly in all directions. In the instrument itself, a laser beam is directed toward the analysed solution and the light is scattered in all directions and detected over a set time period. Intensity of the scattered light fluctuates over time with larger particles, which are slower, showing slower fluctuations and higher amplitudes of scattering

intensities than smaller particles. Detected signal is then used for determination of the hydrodynamic diameter of the particles. DLS provides information regarding mean size, size distribution and polydispersity of particles in solution. Characterization of IO NPs (dispersed in chloroform) and functionalised and unfunctionalised IO@MS NPs (dispersed in ethanol) was performed using the VASCO^{TM} DL 135 particle size analyzer (Cordouan Technologies).

Transmission electron microscope (TEM) is a widely used tool for obtaining high-resolution two-dimensional images of the sample for its morphological, compositional and crystallografic characterisation. High-energy beam of electrons passes through multiple electromagnetic lenses, strikes the sample and a part of it which is transmitted is further focused by the objective lens into an image. The image consists of darker and lighter areas with dark areas representing the areas electrons are less transmitted through. Samples of IO NPs and IO@MS NPs were deposited onto the copper grids. Images were obtained using a JEM 1400 Plus (JEOL) microscope.

Thermogravimetric analysis (TGA) is an analytical technique used for determining thermal stabilities, oxidative stabilities and compositional properties of materials. The method is based on monitoring the change in weight of a sample that is heated at constant rate in controlled atmosphere. The heated sample usually loses weight due to decomposition, reduction, or evaporation. Functionalised IO@MS NPs were vacuum-dried before the analysis. TGA was performed with Simultaneous thermal analyzer 409 PC/PG (NETZCH), from 20⁰C to 1000⁰C.

2.3. Synthesis of iron oxide nanoparticles with iron (II) stearate as a precursor

The mixture of 1.85 g of iron (II) stereate, 0.5335 g of dibenzyl ether, 1.89 g of oleic acid and 15.80 g of squalane was first heated up to 120⁰C, under stirring for 1 h under in order to remove water. Then, the reaction was put under reflux for 1 h at 350⁰C (Ménard, 2017).

After reaction, mixture was cooled and chloroform and hot acetone were added in 1 to 5 ratio. The suspension was sonicated and centrifuged at 20 krpm 5 min. Than, black precipitate was washed, sonicated and centrifuged with chloroform and hot acetone 11 times using 1 to 7.5 ratio, once using 1 to 4 ratio and once with diethyl ether and ethanol in 1 to 1 ratio. Then, 100 µL of oleylamine was added and one more washing step was performed using chloroform and

acetone in 1 to 3 ratio. The solution was sonicated and centrifuged at 20 krpm 5 min and collected black precipitate of IO NPs was dispersed in 15 mL of chloroform.

2.4. Synthesis of iron oxide nanoparticles with iron (III) oxide as a precursor

A mixture of 0.18 g of hydrated iron (III) oxide, 5 g of docosane and 3,2 g of oleic acid was heated up to 50ºC and stirred first under vacuum for 30 min, and then under argon flow for additional 30 min. The temperature was then increased to 350ºC and the reaction was kept at this temperature under reflux and argon flow for 90 min.

After reaction, mixture was slowly cooled to 50ºC and 15 mL of pentane, 20 mL of ethanol and 10 mL of diethyl ether were added. This suspension was ultrasonically dispersed and centrifuged (20 000 rpm, 10 min). The black precipitate was washed two times: once with 2 mL of pentane, 20 mL of ethanol and 10 mL of diethyl ether and once with 15 mL of ethanol and 15 mL of diethyl ether. Finally, nanoparticles were redispersed in 15 mL of chloroform and 200 µL of oleylamine was added in order to stabilize the solution (Nyalosaso et al., 2016).

2.5. Iron oxide/mesoporous silica core-shell nanoparticles

2.5.1. Synthesis of core-shell nanoparticles

First, 50 mL of demineralised water were added to 500 mg of CTAB. Then, the solution was heated to 70ºC and kept at that temperature for 1 h while stirring until complete dissolution of the surfactant. After that, 1 mL of IO NPs dispersed in chloroform was slowly added to aqueous solution and stirred at room temperature for 30 min. The emulsion was then heated to 70ºC in order to evaporate chloroform (10 to 15 min). Then, the solution was diluted with 150 mL of demineralised water containing 60 µL of NaOH (2 M) and 1.5 mL of TEOS and 2.5 mL of ethyl acetate were subsequently added to the mixture. This reaction was then stirred for 3 h at 70 ºC (Ménard et. al., 2019).

2.5.2. Washing of core-shell nanoparticles

After the synthesis, IO@MS NPs have to be washed from residual reactants in order to stop the reaction as well as residual surfactant molecules. First, the mixture was centrifuged at 20 000 rpm for 10 min. Then, the collected precipitate was washed, sonicated and centrifuged (20 krpm, 10 min) several times with ethanol and/or demineralised water. When the foaming of the suspension in water is no longer observed, it was an indication that the IO@MS NPs had been sufficiently washed from free surfactant molecules but this had to be confirmed by IR spectroscopy.

Then, CTAB extraction was performed according to the following protocol adapted from Lang and Tuel (2004). First, IO@MS NPs were dispersed in an ethanolic solution (95%) of ammonium nitrate (10 g L^{-1}), heated up to 62ºC and stirred for 1 h. The extraction was followed by centrifugation (20 krpm, 10 min) and washing of the precipitate with ethanol and/or demineralised water. CTAB extraction has to be performed at least 2 times after the synthesis of IO@MS NPs.

2.6. Surface functionalization of core-shell nanoparticles

3 separate batches of sufficiently washed IO@MS NPs were functionalized with alkoxysilylated DTPA according to the following protocol adapted from Dib et. al. (2014). First, a ligand solution was prepared. The solution consisted of DTPA dianhydride (2, 6 or 10 mmol DTPA dianhydride/g IO@MS NPs), 35.4 mg of APTES, 16.2 mg of triethylamine and 4 mL of dimethylformamide and was sonicated for 20 min and stirred for 3 h at the room temperature. IO@MS NPs were sonicated in 4 mL of absolute ethanol for 10 min, and then the ligand solution was added. The whole volume was heated up to 70ºC for 24 h. Then, the solution was centrifuged for 10 min at 21 000 rpm and the precipitate was washed, sonicated, and centrifuged (21 krpm, 10 min) once with absolute ethanol, twice with demineralised water and once with acetone. Finally, functionalised IO@MS NPs were redispersed in absolute ethanol.

3. RESULTS AND DISCUSSION

3.1. Iron oxide nanoparticles

IO NPs synthesised by thermal decomposition method with iron (II) stearate as a precursor were first imaged by TEM. As observed in Figure 4, the samples are very polydispersed in size and shape. Batch IO-02 (Figure 4a) has two populations: one are IO NPs with spherical morphology and average size around 21 nm and the second one is made of small, irregularly shaped nanoparticles with average size around 10 nm with some as small as 5 nm. Batch IO-03 (Figure 4b) is more monodispersed in size with average size around 11 nm. Still there are very small particles with size around 5 nm. Most of them are irregularly shaped with small percentage of triangle-shaped nanoparticles. Batch IO-04 (Figure 4c) is the most polydispersed. Size range of these nanoparticles is from around 5 nm to 25 nm. There are iregularly-shaped nanoparticles, spherical and triangle shaped nanoparticles. Morphological differences observed from one batch to another may be due to the limitation of equipment. Indeed, the temperature of the reaction couldn't be controled as precisely as it was possibly needed which led to batches not having identical temperature profile during the synthesis. It can be concluded that the protocol used has bad reproducibility.
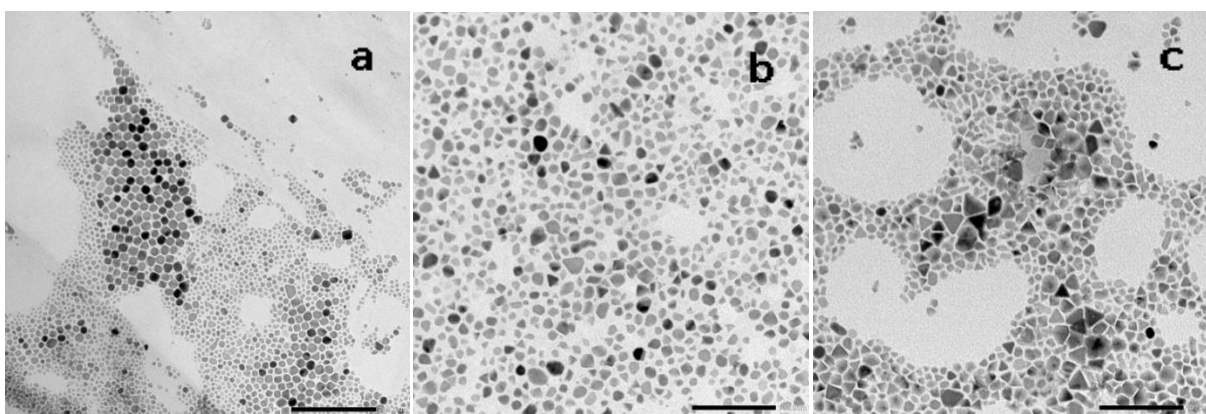

Figure 4. TEM images of three batches of IO NPs obtained according to the protocol described in 2.3.: a – IO-02, b – IO-03, c – IO-04

IO NPs were characterised by IR spectroscopy. According to the Figure 5a, we can differentiate: absorption bands at 2915 cm^{-1} and 2848 cm^{-1} which correspond to asymmetric and symmetric streaching of the CH$_2$ from both oleic acid and stearate chains, absorption bands at 1554 cm^{-1} and 1419 cm^{-1} which correspond to COO$^-$ asymmetric and symmetric streaching vibrations from oleic acid grafted onto the surface of the IO NPs, absorption band at 1135 cm^{-1} which corresponds to C-O bond, absorption bands at 717 cm^{-1} and 697 cm^{-1} that correspond to stereate residue and, finally, absorption bands at 620 cm^{-1} and 571 cm^{-1} which correspond to Fe-O bond. Purification of the IO NPs was monitored by following the ratio of the intensities of absorption bands at 2915 cm^{-1} and 571 cm^{-1} assuming that if the ratio is around 1, a monolayer of oleic acid is formed around IO NPs and sample is presumed cleaned. Comparing Figure 5a and 5b, much of the progress in purification can't be seen even after 8 washings with chloroform and acetone. Because these washings were ineffective, combination of diethyl ether and hot ethanol was used. In Figure 5c, it can be seen that this washing step was too strong. Beside purification IO NPs of the stereate and excess of oleic acid, according to the ratio of the intensities of absorption bands at 2915 cm^{-1} and 571 cm^{-1} which is too low, it can be concluded that even oleic acid from monolayer around IO NPs was desorbed and washed. In attempt to stabilize IO NPs, 100 µL of oleylamine was added, solution was sonicated in order to improve its adsorption onto the surface and one more washing soft washing with chloroform and acetone was performed to wash the excess of oleylamine (Figure 5d). According to the DLS (Figure 6), the average hydrodynamic diameter according to the Pade-Laplace analysis in volume was around 65 nm so it can be concluded that even though oleylamine was added, it didn't reformed a monolayer around individual IO NPs and thus they stayed aggregated.
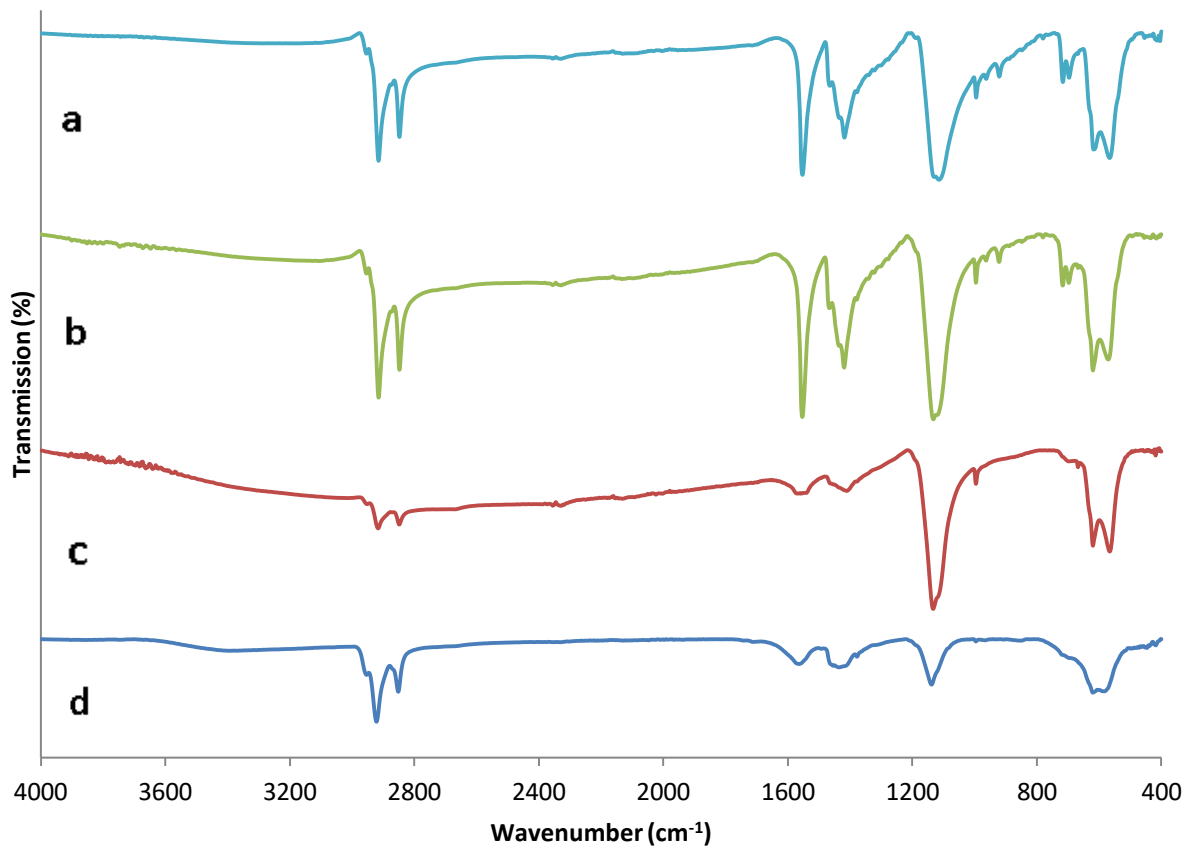
Figure 5. IR spectra of IO NPs after: a - 4 washings with chloroform and acetone (one 1:4 and three 1:7.5), b – 8 more washings with chloroform and acetone (1:7.5), c – 1 more washing with chloroform and acetone (1:4) and 1 washing with diethyl ether and ethanol (1:1), d – addition of 100 µL of oleylamine and 1 more washing with chloroform and acetone (1:3)
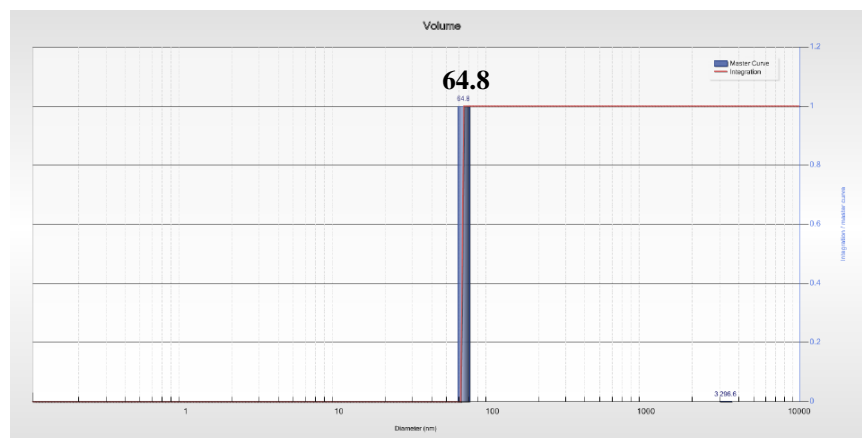
Figure 6. DLS analysis of sample IO-03

IO NPs synthesised by thermal decomposition method with iron (III) oxide as a precursor were first imaged by TEM. Monodispersity of the size and shape of nanoparticles synthesised according to this protocol can be observed in Figure 7.
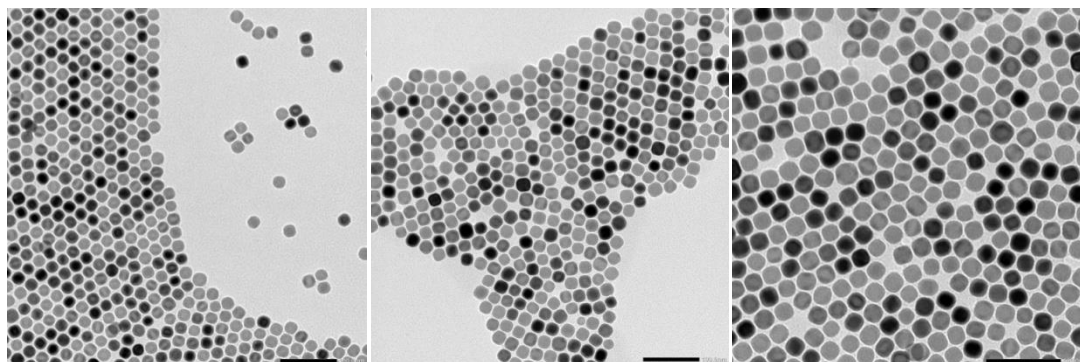

Figure 7. TEM images of IO NPs synthesised according to the protocol described in 2.4.

Size analysis of 100 nanoparticles per sample using the TEM images (Table 1) and representation of narrow size distribution by histograms (Figure 8) are evidence of high reproducibility of used protocol (average diameter of IO NPs synthesised using iron (III) oxide is ranging from 22 nm to 25 nm). Results of DLS analysis are shown in Table 1. Average

hydrodynamic size of samples ranging from 22 nm to 27 nm for the IO NPs dispersed in EtOH (Pade-Laplace in volume analysis) confirms TEM size analysis. This narrow DLS size distribution also proves that there is no aggregates and that the nanoparticles are stable in solution .

Table 1. Size analysis of IO NPs

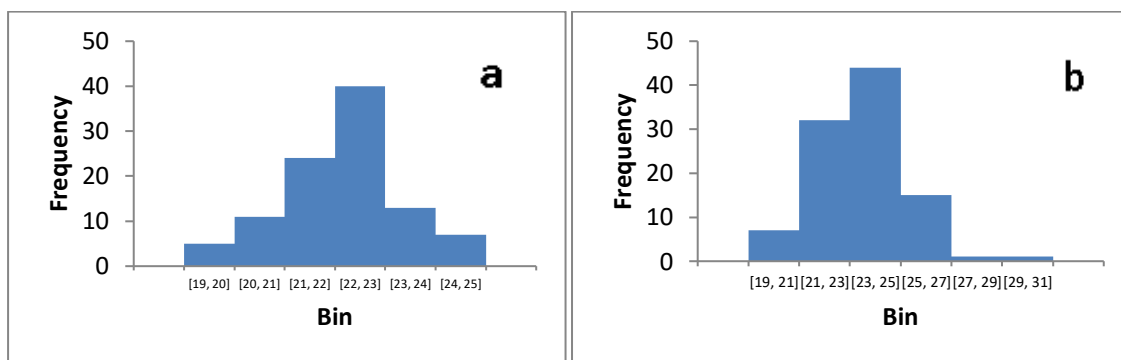| SAMPLE	PRECURSOR USED FOR IO NPs SYNTHESIS	d_{TEM} [nm]	AVERAGE HYDRODINAMIC DIAMETER (DLS) (nm)	PDI
IO-01	iron (III) oxide	24 ± 2	23,41	0.07649
IO-06	iron (III) oxide	25 ± 2	22,36	0.15178
IO-07	iron (III) oxide	22 ± 1	26,90	0.17638
IO-08	iron (III) oxide	23 ± 2	23,41	0.12539

Figure 8. Histograms of the samples IO-07 (a) and IO-08 (b)

IO NPs obtained through protocol described in 2.4. were also characterized by IR spectroscopy (Figure 9). The absorption bands at 2923 cm^{-1} and 2853 cm^{-1} correspond to asymmetric and symmetric streaching of the CH$_2$ from oleic acid respectively. The absorption bands at 1546 cm^{-1} and 1410 cm^{-1} correspond to COO$^-$ asymmetric and symmetric streaching

vibrations from oleic acid grafted onto the surface of the IO NPs. The bond at 558 cm-1 corresponds to Fe-O bond in the iron oxide. Adding of oleylamine is evident through increased intensities of absorption bands at 1546 cm^{-1} and 1410 cm^{-1} in correlation to absorption bonds at 1546 cm^{-1}, 1410 cm^{-1} and 558 cm^{-1} and appeareance of the absorption band at 3320 cm^{-1} which corresponds to N-H bond in oleylamine.
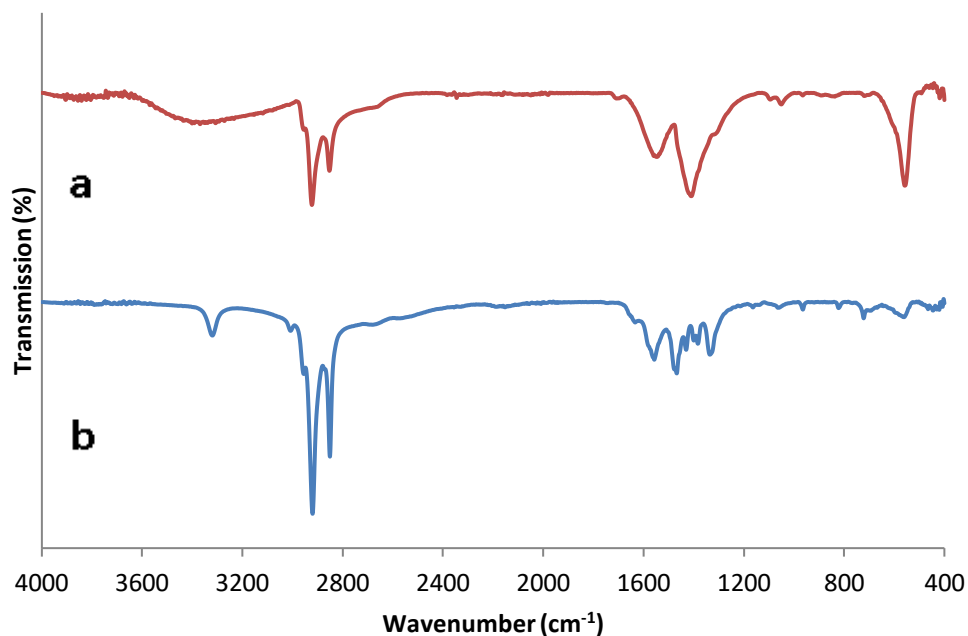

Figure 9. IR spectra of IO@MS NPs before (a) and after (b) addition od oleylamine

3.2. Core-shell nanoparticles

IO@MS NPs were synthesised according to the protocol described in 2.5. using both types of IO NPs as cores. The resulting IO@MS NPs were imaged by TEM (Figure 10).
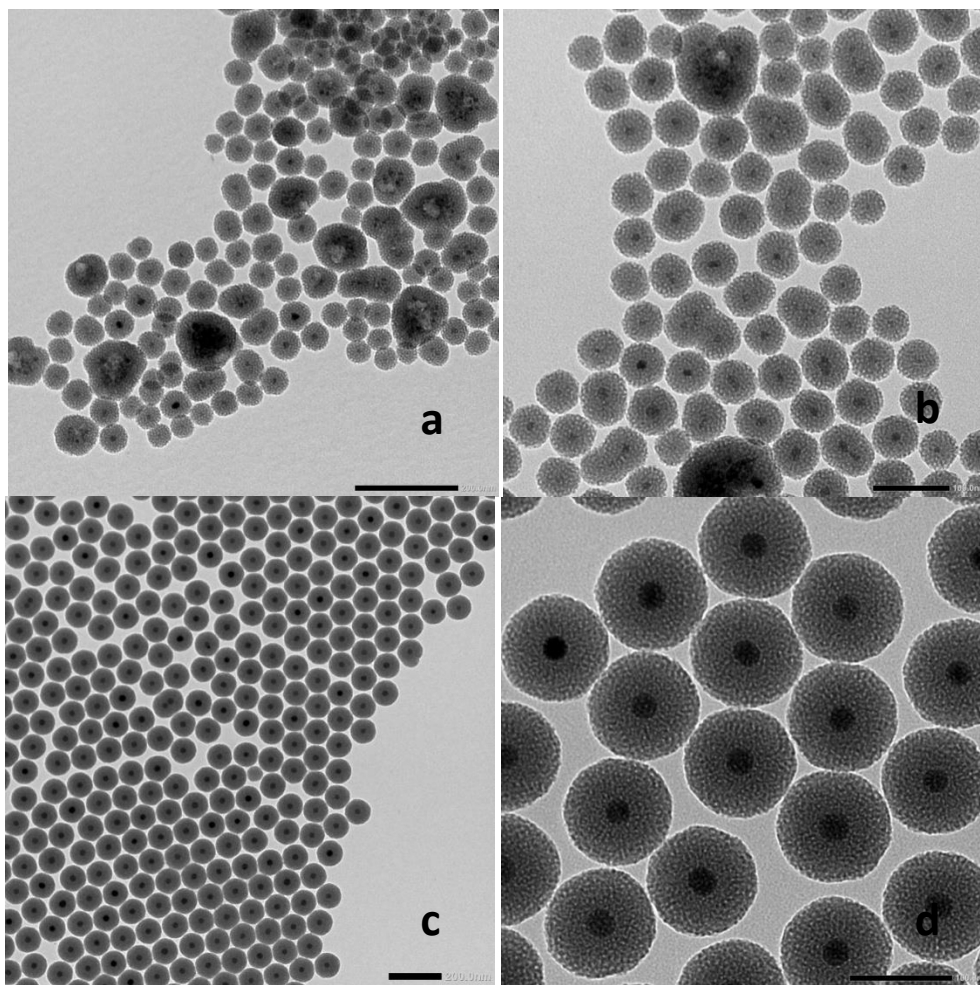
Figure 10. TEM images of IO@MS NPs: a and b – IO@MS NPs with cores synthesised using the iron (II) stearate as a precursor, c and d – IO@MS NPs with cores synthesised using the iron (III) oxide as a precursor

According to the TEM images, IO@MS NPs containing the iron oxide cores synthesised using the iron (II) stearate as a precursor are polydisperse in size and shape. Size analysis of TEM images evidenced an average size of 60 nm (Table 2). On the other hand, histogram (Figure 11) gives representation of size polydispersity in the sample with the presence of the large nanoparticles around 118 nm in diameter. This could be partially explained by the initial polydispersity of IO NPs used as cores in sol-gel process. This could also be due to a non-negligible aggregation of IO NPs caused by too strong purification process. When these aggregates are are used as core in the sol-gel process, this can lead to larger nanoparticles with

multiple cores (Figure 10a and 10b) and/or lower yield of the process. Indeed, aggregated IO NPs are not well stabilised with oleic acid during the phase transfer so when the organic phase evaporates, nanoparticles aggregate which leads to sedimentation on bottom of the glassware or deposition onto the magnetic stirrer. Final product also showed to be less attracted by magnet than expected which might be explained by the fact that the layer of silica is covering iron oxide core and/or the possibility that the highly magnetic IO NPs in polydispersed sample were attracted by the magnetic stirrer which left only smaller, less magnetic iron oxide nanoparticles disposable for sol-gel process. Final product was also characterised by DLS (Figure 12) which shows presence of aggregates in the sample.

Table 2. Size analysis of IO@MS NPs

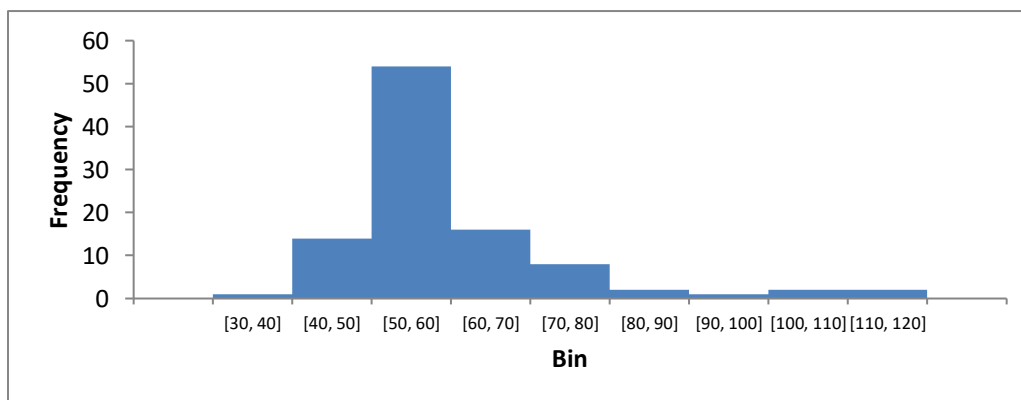| SAMPLE	PRECURSOR USED FOR IO NPs SYNTHESIS	d_{TEM} [nm]
MCS-31	iron (II) stearate	60 ± 15
MCS-61	iron (III) oxide	100 ± 11
MCS-62	iron (III) oxide	101 ± 8
MCS-63	iron (III) oxide	105 ± 6
MCS-64	iron (III) oxide	107 ± 6

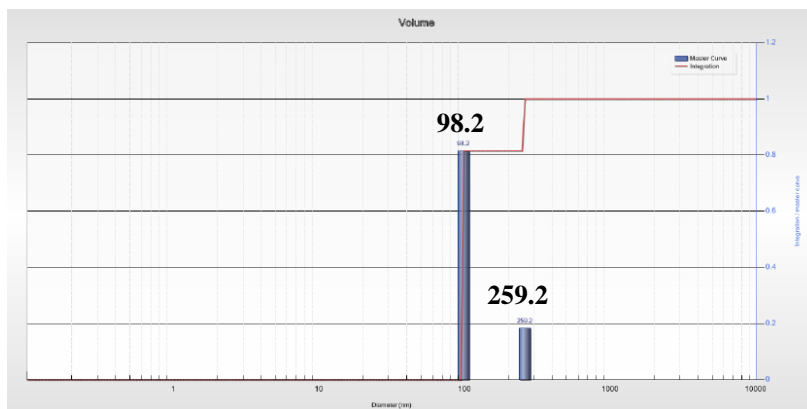**Figure 11.** Histogram of the sample MCS-31

Figure 12. DLS of the sample MCS-31

According to the Figure 10c and 10d, IO@MS NPs obtained using for cores IO NPs synthesised with iron (III) oxide as precursor, are spherical, monodispersed nanoparticles. Size analysis of the TEM images gives the IO@MS NPs the average size of around 105 nm and the histograms of two samples (Figure 13) prove that the size range is narrow with very little frequency of multicore (usually larger IO@MS NPs) or nanoparticles without cores (usually smaller IO@MS NPs). According to DLS analysis (Figure 14) there are very none or very little aggregation in these samples.
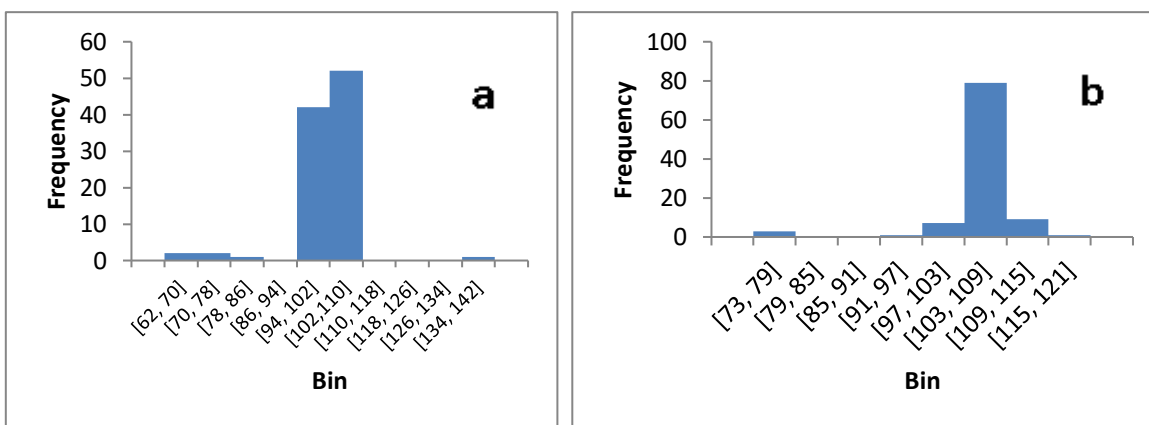

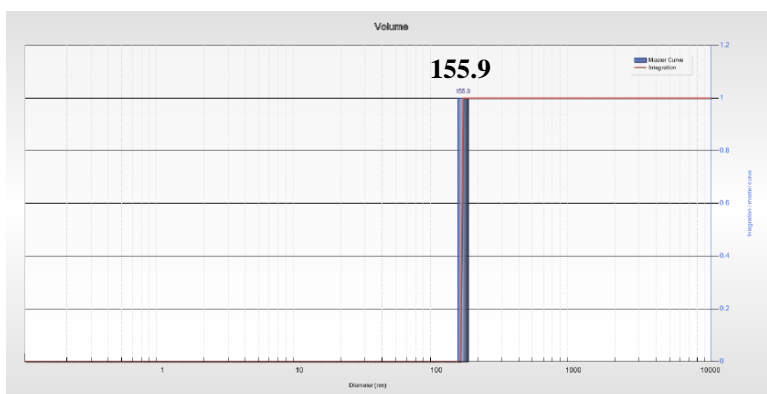**Figure 13.** Histograms of the samples MCS-62 (a) and MCS-63 (b)

Figure 14. DLS of the sample MCS-62

Monodispersity of the product, easier washing steps and higher yield were the reasons of focusing on the IO@MS NPs synthesised using the IO NPs obtained with iron (III) oxide. The downside to these nanoparticles is that they are not magnetic enough, i.e. not attracted by a magnet. Assuming that this low magnetic attraction due to low oxidation of the iron oxide cores, an experiment was set that aimed to find out whether the better oxidation of the iron oxide cores could be achieved through prolonging the time of phase transfer in sol-gel process. If successful, the experiment would result in more magnetic IO@MS NPs. For this purpose, three batches of IO@MS NPs were synthesised by varying the phase transfer time: 1 h, 2 h and 3 h respectively. After the synthesis and the washing steps, the IO@MS NPs dispersed in ethanol were put in transparent plastic cuvettes near the magnet and the attraction time was mesured. The experiment was stopped after 1 hour. Only sample with phase transfer of 1 h was attracted by the magnet: after 10 minutes almost all IO@MS NPs were attracted by the magnet (Figure 15). On the contrary, 2 h and 3 h samples were showing no attraction by the magnet after 1 h. This can probably be explained by the fact that 1 h sample consisted mostly of aggregated nanoparticles which are more attracted by the magnet than nanoparticles that are individually dispersed and these aggregates couldn't be broken down even by sonication for a long period of time. The aggregation of the core-shell nanoparticles can be observed by DLS in Figure 16. After this test, it could be said that prolonging the phase-transfer time during sol-gel process doesn't affect magnetic properties of the IO@MS NPs whereas the aggregation state of nanoparticles has a strong effect on their magnetic attraction.
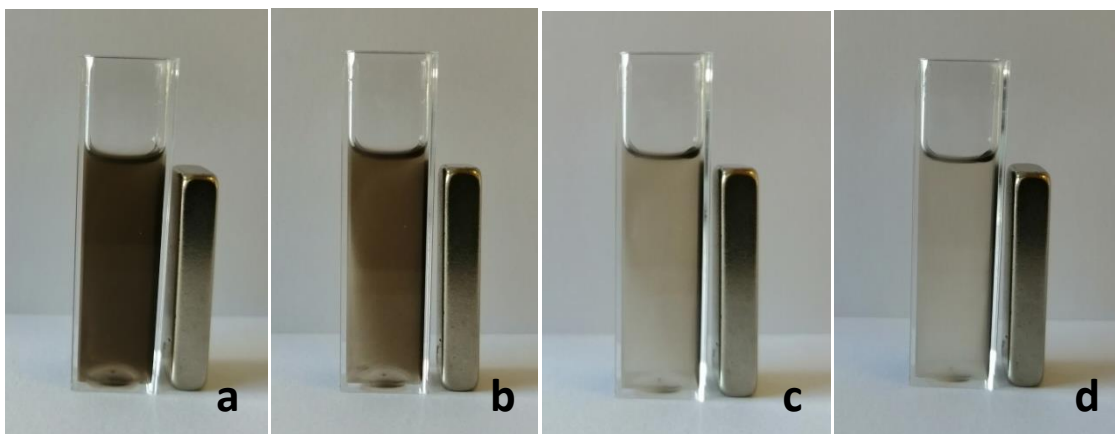
Figure 15. IO@MS NPs synthesised with phase transfer of 1 h (a – start, b - after 2 minutes, c – after 5 minutes, d - after 10 minutes)
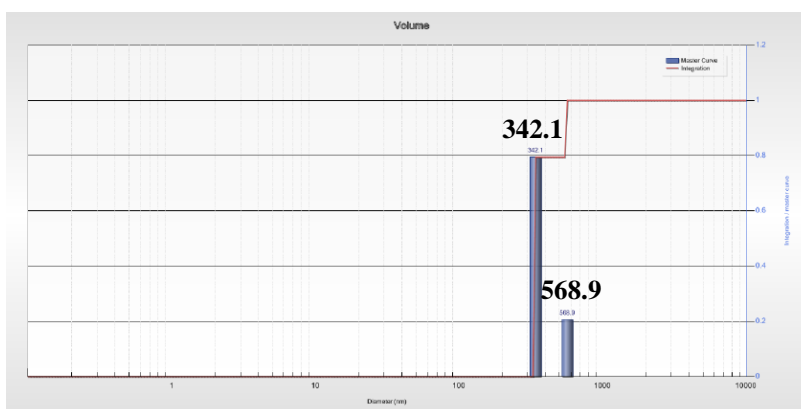

Figure 16. DLS of the sample MCS-1h

Before their functionalization, IO@MS NPs have to be purified which includes washing with water and/or ethanol and extraction of the surfactant (CTAB). Figure 17 shows IR spectra of incompletely and satisfyingly washed IO@MS NPs. The absorption bands that are followed are at 2901 cm^{-1} and 2988 cm^{-1} and they correspond to symmetric and asymmetric streaching of the CH$_2$ from CTAB. When they completely or almost disappear, the sample is considered sufficiently washed. Band at 1080 cm^{-1} corresponds to asymmetric streching vibrations of Si-O-

Si bond and the one at 965 cm^{-1} correspons to Si-OH streching. The absorption band at 461 cm^{-1} is a result of Si-O-Si vibrations.

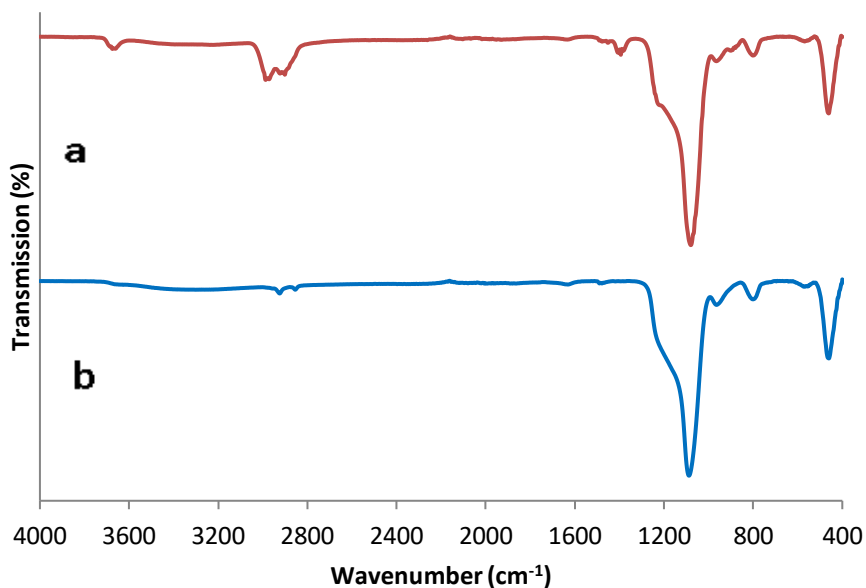**Figure 17.** IR spectra of a – incompletely and b - sufficiently washed IO@MS NPs (washing after second extraction)

3.3. Surface functionalization

IO@MS NPs synthesised using the IO NPs obtained with iron (III) oxide were functionalised with DTPA. Surface of IO@MS NPs was silanized with APTES which provided amine functional groups available for grafting with DTPA dianhydride (Figure 18). Reaction was performed in ethanol.
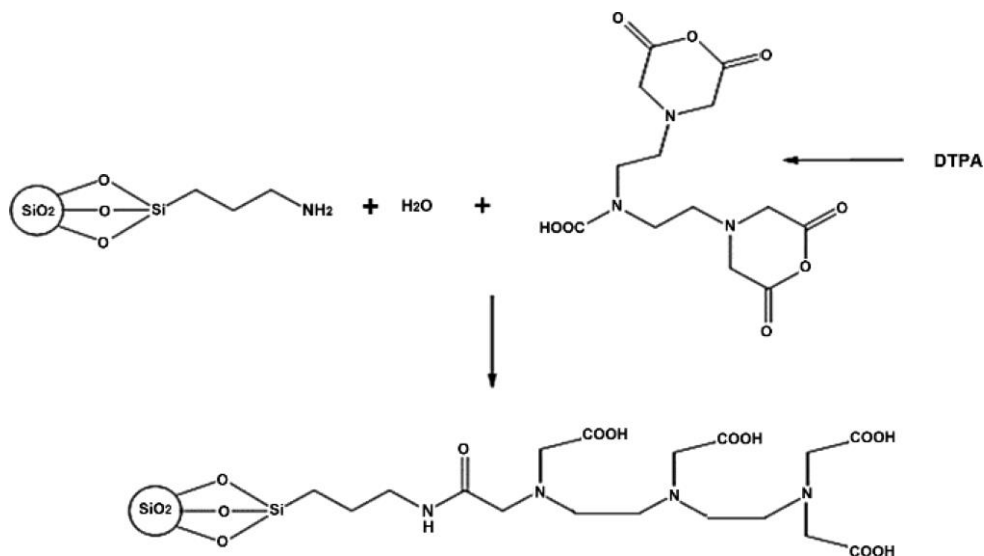
Figure 18. Grafting of DTPA dianhydride on the APTES-functionalised surface (Ashour et al., 2018)

As APTES has only one available functional group for reaction with DTPA dianhydride, for potentially increasing the amount of DTPA grafted onto IO@MS NP, concentration of both APTES and DTPA dianhydride should be increased to preserve 1 to 1 ratio. But the goal of this experiment was to see wether by increasing only the amount of DTPA dianhydride (excessive addition of one reactant) in regards to IO@MS NPs mass, it will improve the efficacy of the grafting process.

After the functionalization, IO@MS NPs were characterised by IR spectroscopy and DLS. According to the Figure 19, grafting of DTPA was successful which can be seen by the appearance of absorption band at 1650 cm^{-1} which corresponds to C=N and the one at 1392 cm^{-1} which corresponds to N-C bond. The grafting was also confirmed by DLS (Figure 20). According to the Pade-Laplace analysis in volume, average hydrodynamic diameter was increased from 82 nm for unfunctionalised to 259 nm for functionalised IO@MS NPs.
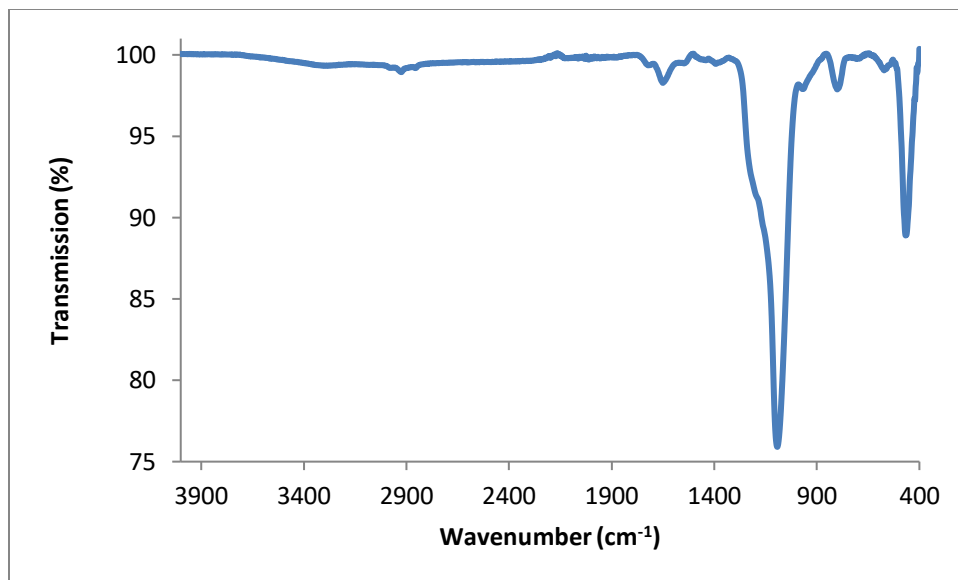
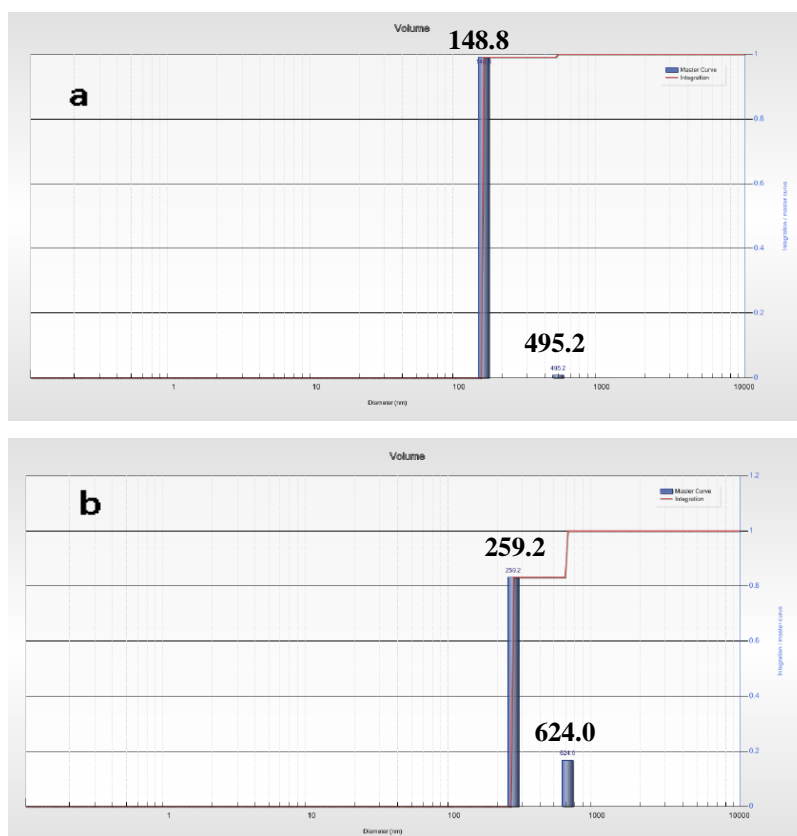**Figure 19.** IR spectrum of functionalised IO@MS NPs

Figure 20. DLS analysis for (a) unfunctionalised and (b) functionalised IO@MS NPs

All three samples were vacuum dried and analysed by TGA (Figure 21) using the temperature range from 20⁰C to 1000⁰C. Final mass loss of the funtionalized IO@MS NP samples, MCS-61, MCS-63 and MCS-64, was 33.61%, 38,09% and 31.03%, respectively. In the range from 20⁰C to 150⁰C, weight loss can be attributed to asdorbed water: 3.82% for sample MCS-61. 3.19% for sample MCS-63 and 3.02% for MCS-64. The rest can be attributed to organic phase of the samples – grafted APTES and DTPA as well as residual CTAB. According to TGA results, it can be concluded that the efficacy of the grafting process isn't increased with the amount of DTPA dianhydride (excessive addition of one reactant) in regards to mass of IO@MS NPs in reaction mixture. For increasing the amount of grafted ligand, amount of APTES should also be increased in the way that ratio of APTES and DTPA dianhydride in reaction mixture is 1 to 1.
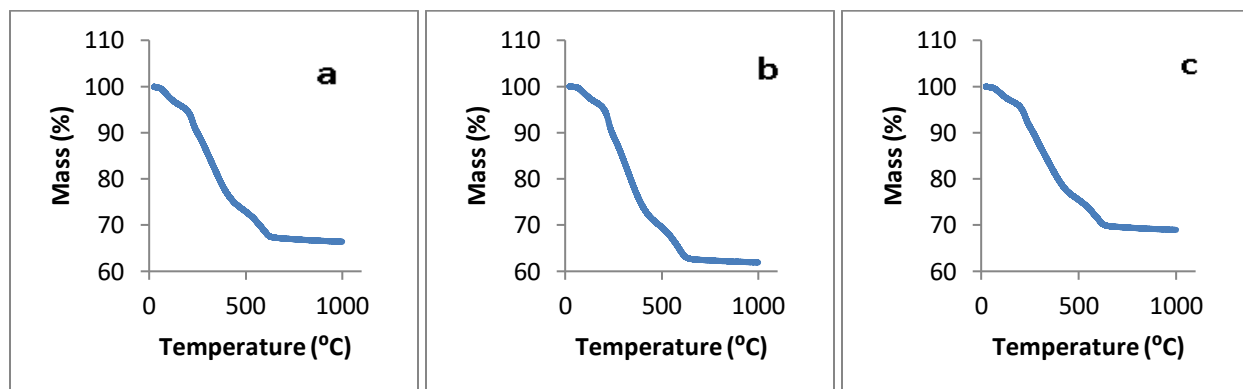

Figure 21. TGA analysis of functionalised IO@MS NPs: MCS-61 (a), MCS-63 (b) and MCS-64 (c)

4. CONCLUSION

In this thesis, I synthesized and functionalised IO@MS NPs. First I synthesised and compared IO NPs obtained with two different protocols. IO NPs synthesised with iron (II) stearate were highly attracted by the magnet but they were also polydispersed in shape and size with protocol itself not giving reproducible results. IO@MS NPs synthesised with these IO NPs were polydispersed in size as well with some of them having multiple cores. It was concluded that washing steps after the synthesis were too strong which led to the aggregation of IO NPs and lower the yield of the sol-gel process than expected. IO NPs synthesised with iron (III) oxide and IO@MS NPs obtained through synthesis with them were monodispersed in shape and size but both showed low attraction by the magnet.

IO@MS NPs synthesised using the IO NPs obtained with iron (III) oxide were sucessfully functionalised with DTPA. Results showed that by increasing only the amount of DTPA dianhydride (and not the amount of APTES) in regards to mass of IO@MS NPs in reaction mixture doesn't improve the efficacy of the grafting process and that 1 to 1 ratio of APTES and DTPA dianhydride is enough for successful functionalization.

To conclude, in order for these nanoparticles to be used in recovering of REEs from aqueous solutions, future work should be aimed towards the optimization of synthesis and washing steps of IO NPs which will be used as cores in sol-gel process and increasing the amount of DTPA grafted onto the surface of IO@MS NPs. Moreover, the toxicity of these functionalised nanoparticles should be tested as well as efficiency of the adsorption of targeted REEs in aqueous solutions.

5. REFERENCES

Abraham I. (2011). Rare earths: The cold war in the annals of travancore. In Hecht G. (Ed.) *Entangled geographies: Empire and technopolitics in the global cold war* (pp. 101-124). Cambridge, London: The MIT Press.

Anastopoulos I., Bhatnagar A. and Lima E. C. (2016). Adsorption of rare earth metals: A review of recent literature. *J. Mol. Liq.* **221**: 954-962.

Arias L. S., Pessan J. P., Vieira A. P. M., Toito de Lima T. M. , Botazzo Delbem A. C. and Monteiro D. R. (2018). Iron oxide nanoparticles for biomedical applications: A perspective on synthesis, drugs, antimicrobial activity, and toxicity. *Antibiotics* **7**: 46.

Ashour R. M., Samouhos M., Polido Legaria E., Svärd M., Högblom J., Kerstin Forsberg K., Palmlöf M., Kessler V. G., Seisenbaeva G. A. and Rasmuson Å. C. (2018). DTPA-Functionalized silica nano- and microparticles for adsorption and chromatographic separation of rare earth elements. *ACS Sustain. Chem. Eng.* **6**: 6889-6900.

Binnemans K. and Jones P. T. (2015). Rare earths and balance problem. *J. Sustain. Metall.* **1(1)**: 23-38.

Bruce I. J. and Sen T. (2005). Surface modification of magnetic nanoparticles with alkoxysilanes and their application in magnetic bioseparations. *Langmuir* **21(15)**: 7029-7035.

Callura J. C., Perkins K. M., Noack C. W., Washburn N. R., Dzombak D. A. and Karamalidis A. K. (2018). Selective adsorption of rare earth elements onto functionalized silica particles. *Green Chem.* **20**: 1515-1526.

Campos E. A., Stockler Pinto D. V. B., Sampaio de Oliveira J. I., da Costa Mattos E. and de Cássia Lazzarini Dutra L. (2015). Synthesis, caracterization and applications of iron oxide nanoparticles – a short review. *J. Aerosp. Technol. Manag.* **7(3)**: 267-276.

Chen Y. and Zheng B. (2019). What Happens after the Rare Earth Crisis: A Systematic Literature Review. *Sustainability* **11(5)**: 1288.

Cornell R. M. and Schwertmann U. (2003). *The iron oxides: Structure, properties, reactions, occurences and uses*, 2nd ed. Weinheim, Berlin, Zurich: Wiley-VCH.

Dib S., Boufatit M., Chelouaou S., Sadi-Hassaine F., Croissant J., Long J., Raehm L., Charnay C. and Durand J.-O. (2014). Versatile heavy metals removal *via* magnetic mesoporous nanocontainers. *RSC Adv.* **4**: 24838-24841.

Fan H. Y., Yang K., Boye D. M., Sigmon T., Malloy K. J., Xu H. F., Lopez G. P. and Brinker C. J. (2004). Self-assembly of ordered, robust, three-dimensional gold nanocristal/silica arrays. *Science* **304(5670)**: 567-571.

Fan H., Leve E. W., Scullin C., Gabaldon J., Tallant D., Bunge S., Boyle T., Wilson M. C. and Brinker C. J. (2005a). Surfactant-assisted synthesis of water-soluble and biocompatible semiconductor quantum dot micelles. *Nano Lett.* **5(4)**: 645-648.

Fan H., Leve E. W., Scullin C., Gabaldon J., Wright A., Haddad R. E. and Brinker C. J. (2005b). Ordered two- and three-dimensional arrays self-assembled from water-soluble nanocrystal–micelles. *Adv. Mater.* **17(21)**: 2587-2590.

Florea N.-M., Lungu A., Vasile E. and Iovu H. (2013). The influence of nanosilica functionalization on the properties of hybrid nanocomposites. *High Perform. Polym.* **25(1)**: 61–69.

Guardia P., Riedinger A., Nitti S., Pugliese G., Marras S., Genovese A., Materia M. E., Lefevre C., Manna L. and Pellegrino T. (2014). One pot synthesis of monodisperse water soluble iron oxide nanocrystals with high values of the specific absorption rate. *J. Mater. Chem. B* **2**: 4426-4434.

Guo WL., Nie CM., Wang L., Li ZJ., Zhu L., Zhu LZ., Zhu ZT., Shi WQ. and Yuan LY. (2016). Easily prepared and stable functionalised magnetic ordered mesoporous silica for efficient uranium extraction. *Sci. China Chem.* **59(5)**: 629-636.

Knezevic N. Z., Mauriello Jimenez C., Albino M., Vukadinovic A., Mrakovic A., Illes E., Janackovic Dj., Durand J.-D., C. and Peddis D. (2017). Synthesis and characterization of core-shell magnetic mesoporous silica and organosilica nanostructures. *MRS Advances, 2***(19-20)**: 1037-1045.

Lang N. and Tuel A. (2004). A fast and efficient ion-exchange procedure to remove surfactant molecules from MCM-41 materials. *Chem. Mater.* **16**: 1961-1966.

Li D., Jiang D., Chen M., Xie J., Wu Y., Dang S. and Zhang J. (2010). An easy fabrication of monodisperse oleic acid-coated Fe_3O_4 nanoparticles. *Mater. Lett.* **64(22)**: 2462-2464.

Ménard M. (2017). Synthesis of hybrid core-shell nanoparticles for theranostic applications (Doctoral dissertation). Retrieved from The Center for Direct Scientific Communication. (HAL Id: tel-01820658, version 1)

Ménard M., Meyer F., Affolter-Zbaraszczuk C., Rabineau M., Adam A., Duenas Ramirez P., Bégin-Colin S. and Mertz D. (2019). Design of hybrid protein-coated magnetic core-mesoporous silica shell nanocomposites for MRI and drug release assessed in a 3D tumor cell model. *Nanotechnology* **30(17)**: 174001.

Nyalosaso J. L., Rascol E., Pisani C., Dorandeu C., Dumail X., Maynadier M., Gary-Bobo M., Lai Kee Him J., Bron P., Garcia M., Devoisselle J. M., Prat O., Guari Y., Charnay C. and Chopineau J. (2016). Synthesis, decoration, and cellular effects of magnetic mesoporous silica nanoparticles. *RSC Adv.* **6**: 57275-57283.

Owens G. J., Singh R. K., Foroutan F., Algaysi M., Han C.-M., Mahapatra C., Kim H.-W. and Knowles J. C. (2016). Sol-gel based materials for biomedical applications. *Prog. Mater. Sci.* **77**: 1-79.

Roosen J., Spooren J. and Binnemans K. (2014). Adsorption performance of functionalized chitosan-silica hybrid materials toward rare earths. *J. Mater. Chem. A* **2**: 19415-19426.

Sadegh H., Ali G. A. M., Gupta V. K., Makhlouf A. S. H., Shahryari-ghoshekandi R., Nadagouda M. N., Sillanpää M. and Megiel E. (2017). The role of nanomaterials as effective adsorbents and their applications in wastewater treatment. *J. Nanostructure Chem.* **7(1)**: 1-14.

Swaim N. and Mishra S. (2019). A review on the recovery and separation of rare earths and transition metals from secondary resources. *J. Clean. Prod.* **20**: 884-898.

UNCTAD (2014). Commodities at a glance, Special issue on rare earths. UNCTAD - United Nations Conference on Trade and Development, New York and Geneva.

Wang S., Lu W., Tovmachenko O., Yu H. and Ray P. C. (2008). Challenge in understanding size and shape dependent toxicity of gold nanomaterials in human skin keratinocytes. *Chem. Phys Lett.* **463(1-3)**: 145-149.

Wu W., Wu Z., Yu T., Jiang C. and Kim W.-S. (2015). Recent progress on magnetic iron oxide nanoparticles: synthesis, surface functional strategies and biomedical applications. *Sci. Technol. Adv. Mater.* **16**: 023501.

Yanfei X., Li H., Zhiqi L., Zongyu F. and Liangshi W. (2016). Adsorption ability of rare earth elements on clay minerals and its practical performance. *J. Rare Earth.* **34(5)**: 543-548.

Ye F., Laurent S., Fornara A., Astolfi L., Qin J., Roch A., Martini A., Toprak M. S., Muller R. and Muhammed M. (2012). Uniform mesoporous silica coated iron oxide nanoparticles as a hig hly efficient, nontoxic MRI T_2 contrast agent with tunable proton rel axivities. *Contrast Media Mol. I.* **7**: 460-468.

Zhang L., He R. and Gu H.-C. (2006). Oleic acid coating on the monodisperse magnetite nanoparticles. *Appl. Surf. Sci.* **253(5)**: 2611-2617.

Zhang L., Qiao S., Jin Y., Yang H., Budihartono S., Stahr F., Yan Z., Wang X., Hao Z. and Lu G. Q. (2008). Fabrication and size-selective bioseparation of magnetic silica nanospheres with highly ordered periodic mesostructure. *Adv. Funct. Mater.* **18(20)**: 3203-3212.

Zhanheng C. (2011). Global rare earth resources and scenarios of future rare earth industry. *J. Rare Earth.* **29(1)**: 1-6.

Zhou B., Li Z. and Chen C. (2017). Global potential of rare earth resources and rare earth demand from clean technologies. *Minerals* **7(11)**: 203.

Zhou B., Li Z., Zhao Y., Zhang C. and Wei Y. (2016). Rare Earth Elements supply vs. clean energy technologies: new problems to be solve. *Gospod. Surowcami. Min.* **32(4)**: 29-44.

Zhu M., Lerum M. Z. and Chen W. (2012). How to prepare reproducible, homogeneous, and hydrolytically stable aminosilane-derived layers on silica. *Langmuir* **28(1)**: 416–423.

6. ANNEX

6.1. List of abbreviations

APTES	(3-aminopropyl)trietoxysilane
CTAB	cetyltrimethylammonium bromide
DLS	dynamic light scattering
DTPA	diethylenetriaminepentaacetic acid
IO NPs	iron oxide nanoparticles
IO@MS NPs	iron oxide/mesoporous silica nanoparticles
IR	infrared
TEM	transmission electron microscope
TEOS	tetraethyl orthosilicate
TGA	thermogravimetric analysis

STATEMENT OF ORIGINALITY

This is to certify, that the intellectual content of this thesis is the product of my own independent and original work and that all the sources used in preparing this thesis have been duly acknowledged.

VALENTINA FIŽULIĆ

Name of student